Available online at www.sciencedirect.com

ScienceDirect

Ceramics International 39 (2013) 9447–9457

CERAMICS INTERNATIONAL

www.elsevier.com/locate/ceramint

Spray drying of nanometric SYSZ powders to obtain plasma sprayable nanostructured granules

Mohammad Reza Loghman-Estarki[a,*], Hossein Edris[a], R. Shoja razavi[b], Hossein Jamali[b], Reza Ghasemi[b], Mousa Pourbafrany[b], Mohammad Erfanmanesh[b], Mazaher Ramezani[a,b]

[a]Department of Materials Engineering, Isfahan University of Technology, Isfahan, P. O. Box. 84156-83111, Islamic Republic of Iran
[b]Department of Material Engineering, Malek Ashtar University of Technology, Isfahan, Shahin-shahr, Islamic Republic of Iran

Received 13 March 2013; received in revised form 30 April 2013; accepted 1 May 2013
Available online 30 May 2013

Abstract

This study addresses the correlation between the feedstock agglomerates with their resulting coating microstructure and thermal insulation capability. To this end, the Y_2O_3 and Sc_2O_3 codoped in ZrO_2 (SYSZ) nanopowders were synthesized by the polymeric sol–gel method, their suspensions were agglomerated into plasma sprayable feedstock by the spray drying method, and finally, the effect of feedstock morphology on the microstructures and thermal insulation capability of APS coatings was investigated. The coating microstructure consisted of semi-molten feedstock agglomerates surrounded by fully molten particles that acted as binders. Solid irregular SYSZ granules yielded coatings with lower porosity and thermal insulation capability than the porous spherical YSZ ones.

Keywords: Granules; APS; Agglomerate; Nanostructure; Plasma sprayable feedstocks; Spray drying

1. Introduction

Granulation is an essential step to improve the flowability of submicrometre and nanometric ceramic powders to make them suitable for thermal spray coatings. Thermal barrier coatings (TBCs) consist of a ceramic top coat made of yttria partially stabilized zirconia (YSZ), which is deposited over a metallic bond coat and used in aircraft turbine engines for thermal insulation in hot sections. Their thermal properties are closely related to the microstructure of the ceramic top coat [1–3], which is, in turn, influenced by the ceramic powder and its morphologies. The codoped zirconia with scandia, yttria (SYSZ), is an advanced functional material used for high temperature TBCs. Thermal stability of these ceramics is up to 1400 °C, while phase stability of conventional YSZs is up to 1150 °C [1]. Nanostructured TBCs can have improved mechanical and thermal properties when compared to those researched in conventional coatings. Spraying nanoparticles enables coatings to be manufactured that exhibit different architectures and properties. However, nanoparticles need to be agglomerated to a sprayable size in order to use regular powder feeders [4–12]. Agglomeration generally takes place by spray drying of the nanoparticle suspension and, frequently, thermal treatment of the granules. Spraying nanostructured (spray-dried) agglomerates leads to a two-scale coating structure that basically comprises semi-molten agglomerates (nanozones) surrounded by fully molten agglomerates that act as a binder [6]. Nanostructured, spray-dried feedstock characteristics such as morphology, size, and void content of the agglomerates are critical to achieve this two-scale microstructure and its potential benefits. This is because, depending on feedstock characteristics and spraying conditions, the nanozones that form the coating may continue to be porous like the original feedstock or be much denser. High powder flowability is also required for homogeneous feeding of the plasma flow in order to produce a continuous and constant powder mass flow.

The bad flowability of powdered materials is one of the reasons that make an agglomeration step essential [9–12].

*Corresponding author. Tel.: +98 312 5225041; fax: +98 312 5228530.
E-mail addresses: mr.loghman@ma.iut.ac.ir, loghman57@gmail.com (M.R. Loghman-Estarki).

0272-8842/$ - see front matter © 2013 Elsevier Ltd and Techna Group S.r.l. All rights reserved.
http://dx.doi.org/10.1016/j.ceramint.2013.05.062

In ceramic industries, agglomeration processes like fluidized bed granulation or spray drying are used to generate ceramic material mixtures with improved handling and processing properties from water or solvent based suspensions [12–15].

Among methods of granulation, such as sintering and crushing process (SC) and spray drying (SD), the SD method shows some advantages due to its spherical morphology and good flowability [13,16–19]. The SD method is routinely used as a spray granulation from slurries to obtain powder with various morphologies, depending on operating parameters and suspension formulation. They can be hollow, dense, porous, and spherical most of the time, though some times with a donut shape. The SDP powder is of good flowability and favorable for thermal spraying.

Most studies on TBCs [6–8] that use nanostructured spray-dried feedstock only mention the agglomeration process without providing any details on the nanoparticle suspension preparation, spray drying operation, or thermal treatment of the resulting agglomerates. Thus, the correlation between agglomeration process variables, agglomerate characteristics, and coating microstructure and properties is yet to be established. In the present report, Y_2O_3 and Sc_2O_3 codoped in ZrO_2 nanoparticles, named as SYSZ, was used to obtain granules with suitable density and flowability for plasma spraying by the spray drying and calcination treatment technology. This study also addresses the correlation between the feedstock agglomerates with the resulting coating microstructure and thermal insulation capability.

2. Experimental procedure

2.1. Materials and nanopowder preparation

The SYSZ nanopowders were prepared in large scale by the polymeric route [1]. The suspensions for spray granulation were prepared with demineralized water (resistivity higher than $0.05 \times 106\ \Omega$ cm at 25 °C) and polyvinyl alcohol (PVA, $[CH_2CHOH_n]$, MW = 10000–13000, Merck & Co.). The pH of suspension was evaluated with the Metrohs pH meter (Swiss).

2.2. Fabrication of feedstock

The nano-sized particles had to be granulated to micron-sized granules since they could not be used as sprayable feedstocks directly. When the nanoparticles were prepared, the fabrication of SYSZ feedstock had to be taken out. The instruments used for the fabrication of feedstocks included ball milling (Retsch PM 100, Germany), spray drying chamber and furnace (Nobertherm, German). The process of feedstock preparation was divided into three stages, as shown below.

2.2.1. Ball milling and suspension (slurry) preparation

The SYSZ nanopowders were put into the ball milling (Retsch PM 100, Germany), which contained 30 wt% solid nanopowders and zirconia based balls (the weight of balls to powder was 10:1). After 6 h ball milling, as a typical mixture of the 180 ml deionized water, 20 g SYSZ nanopowders and 5 wt% binders were stirred homogenously for 2 h. So, the solid loading in suspension are 10 wt%. Furthermore, the same suspension was prepared with as-obtained SYSZ nanopowders without ball milling. The slurry formulation of the second suspension was similar to the previous one.

2.2.2. Spray drying process

When the SYSZ slurry was prepared, the spray drying process was continued directly in order to avoid the precipitation of slurry. The parameters, especially temperature and feeding rate, had to be controlled strictly to prevent the slurry

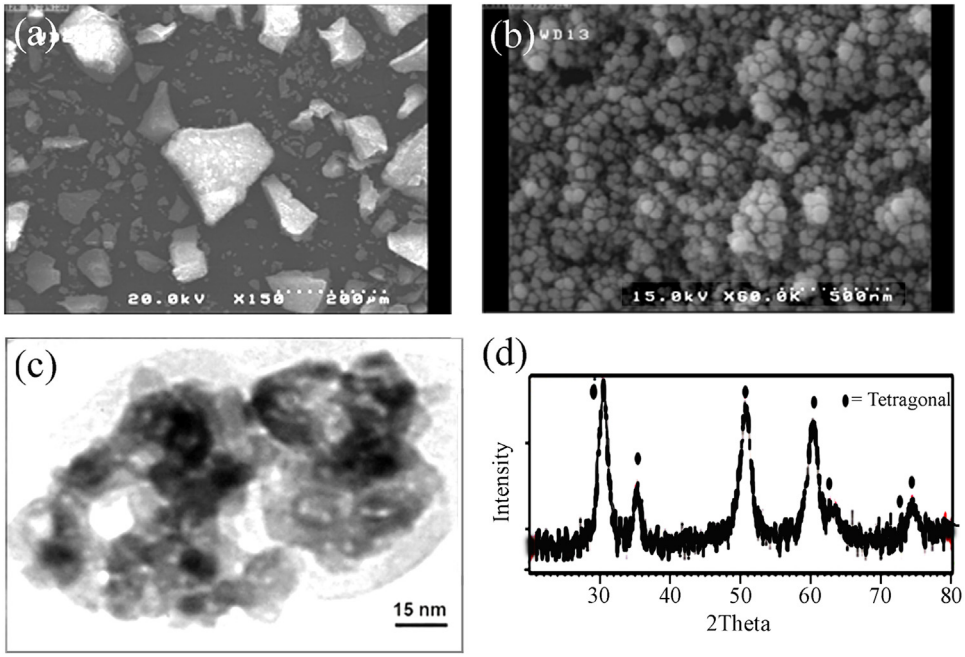

Fig. 1. –>(a) and (b) SEM images, (c) TEM image and (d) XRD pattern of SYSZ nanopowders prepared by the polymeric route.

from sticking to the wall of spray drying chamber. The laboratory spray drying apparatus schematically consisted of a peristaltic pump that fed the slurry into a disc-like atomizer located at the top of the drying chamber and produced a fountain-like spray. The drying air inlet was placed at the top of the chamber so that the initial droplet air mixing was counter-current and then co-current. The solid aggregates were collected at the bottom of the chamber and separated from the gas in cyclone collectors. The main controlled operating parameters were the air temperature at the entry (220–235 °C), at the exit (135–140 °C), inside the chamber (170 °C), the rotate speed of atomizer (14000 rpm), and air (4.4–4.6 lit/h) and slurry flow rates (1–1.2 kg/h). These parameters were kept constant for formulation of both slurries.

2.2.3. Thermal treatment process

In order to increase the density of granules and eliminate all the organic additives, the granulated particles, obtained from the spray drying process, were calcined. The sintering temperature was determined by the thermo gravimetric analysis (TGA, Malek Ashtar Company, Iran) method. After that, the feedstock, whose particle size was suitable for plasma spraying, was obtained. However, unignorable problems, such as high porosity, low flowability, and small particle size, existed in the feedstocks, making them unsuitable for direct plasma spraying. So, small ($< 20\ \mu m$) and very large particles ($> 150\ \mu m$) were removed by passing them through a sieve (100 and 500 US mesh) to meet the demands of sprayable feedstocks.

2.3. Characterization of feedstocks

When the feedstocks were prepared, the basic properties of the particles were tested. For example, the evaluation of apparent density and flow rate was performed, according to ASTM nos. B0212-99 and B 213–03 [20] (using the Hall flowmeter funnel) respectively. The granule size distribution was measured by sieving the granules with different meshes. The crystalline phases were obtained by the X-ray diffraction technique (Rigaku D-max C III, Philips, Holland). A field-emission scanning electron microscope (FESEM) was obtained

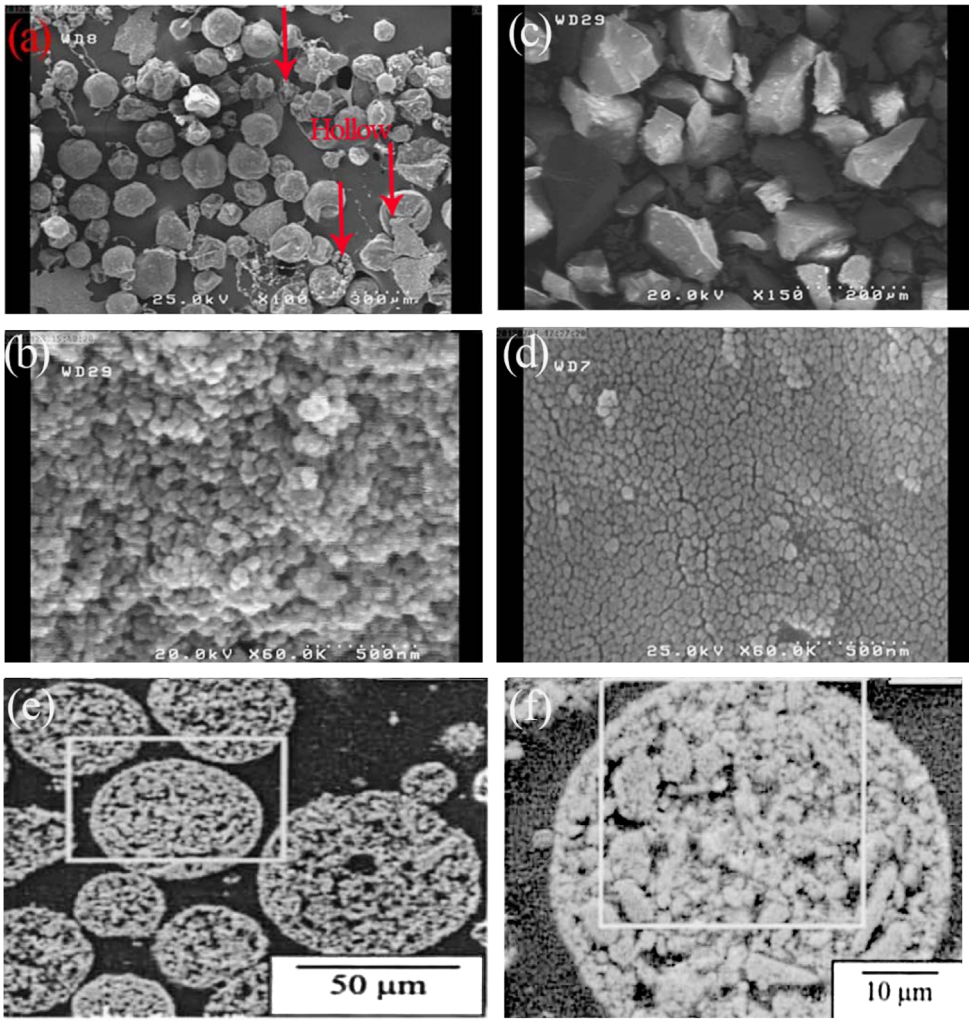

Fig. 2. SEM images of granules obtained from SD2 (a) and (b), SD1 (c) and (d) and (e) and (f) commercial YSZ (Nanox S4007 [6]) nanopowders with different magnifications.

on S-4160 (Hitachi Ltd., Japan). The optical images (OM) were done on OM microscope (Nikon Epiphot 30s, Japan).

2.4. APS coating setup and thermal insulation capability test

The Inconel 738LC Ni-based super alloy was used as the substrate material. Specimens, after grit blasting with Alumina grits mesh 36 and degreasing, were coated with a bond coat of Ni–22Cr–10Al–1Y (wt%) alloy (Amdry 962) by the APS method (Sulzer Metco F4 gun) obtaining a thickness of 100–125 μm. The bond coat powders were sprayed based on the standard parameters recommended by the Sulzer Metco Company [7]. The parameters used to spray the nanostructured SYSZ coating were developed internally (Ar flow = 35 standard liter per minute (slpm), H_2 flow = 10 slpm, arc intensity = 600 A (A), spraying distance = 120 mm, spraying velocity = 1000 mm/min, anode nozzle internal diameter = 6 mm, and feedstock feed rate = 18 g/min).

The coating void contents and semi-molten particle fractions were measured on the cross-sectional coating areas by the image analysis (Image pro-Plus Bethesada MD, USA) of the micrographs obtained by a scanning electron microscope (Philips, Holland) nearby 200, 500 and 1000 magnification. Averages of 10 images, randomly located across the sample, were analyzed for each sample in order to obtain a representative, complete scan of the whole cross-sectional area.

To evaluate thermal insulation value of TBCs, the thermal insulation capability test was done according to our previous report [7]. The schematic illustration of thermal insulation capability test is shown in Refs. [2,7]. Three thermocouples (K type, working temperature up to 1300 °C) were used as sensors, one was located in the furnace to measure the furnace temperatures (T_0) and others were sealed on both sample backsides to monitor the backside temperatures of the coated sample (T_1) and voucher sample (T_2). The thermocouples were linked to thermometer and then computer to record the heating temperature curves (T_0, T_1 and T_2). After installation, the electric furnace was heated to 1000 °C with the average rate of 15 °C/min. To stabilize temperature conditions, the samples were kept in 1000 °C for 40 min. T_0, T_1 and T_2 record from the beginning of the test in 1 min time intervals and t–T curves were plotted. Finally, the thermal insulation capability by the temperature drop across TBC ($\Delta T = T_2 - T_1$) for 20-end data was calculated.

3. Results and discussion

3.1. Characterization of SYSZ nanopowder

Fig. 1a, that shows the SEM image, illustrates the morphology of the SYSZ nanopowder obtained from the polymeric sol–gel method. This sample consisted of relatively compact large particles that showed flat faces and angular edges. This typical morphology was similar to other studies in the literature [1,20,21]. High magnifications of these big facets (Fig. 1b) showed that they consisted of nanometric SYSZ nanoparticles. TEM picture in Fig. 1c shows that the as-prepared samples consisted of crystallites with a size between 30–50 nm. According to XRD pattern (Fig. 1d), the SYSZ nanopowders showed a pure tetragonal phase with cell parameters $a = b = 0.35984$ nm, and $c = 0.50105$ nm.

3.2. Spray drying and calcination process

In order to survey the effect of ball milling treatment on the morphologies of as-prepared granules, FESEM images were taken from them. Fig. 2 shows FESEM micrographs of spray-dried powders for ball milled treated, named as SD1, and non-ball milled (SD2), of SYSZ nanopowder. These powders were obtained from 5 wt% PVA and 10 wt% solid loading in suspensions. Fig. 2a displays the particles morphology of SYSZ suspension with ball milling treatment, after spray

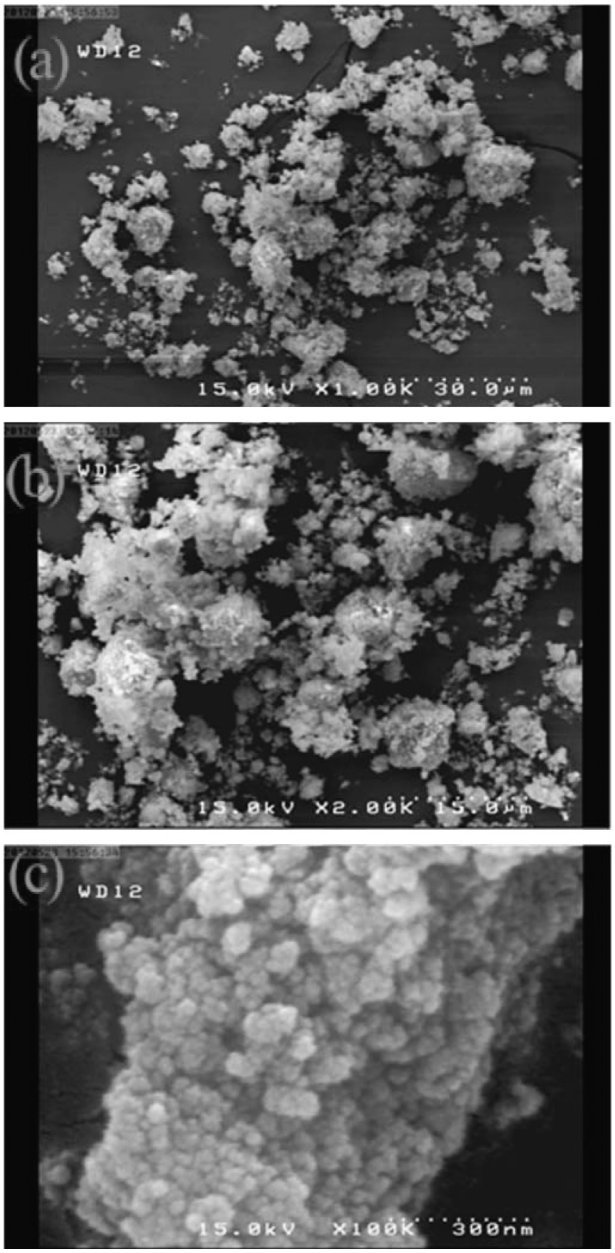

Fig. 3. SEM images (a–c) of SYSZ nanopowders after ball milling process for 6 h.

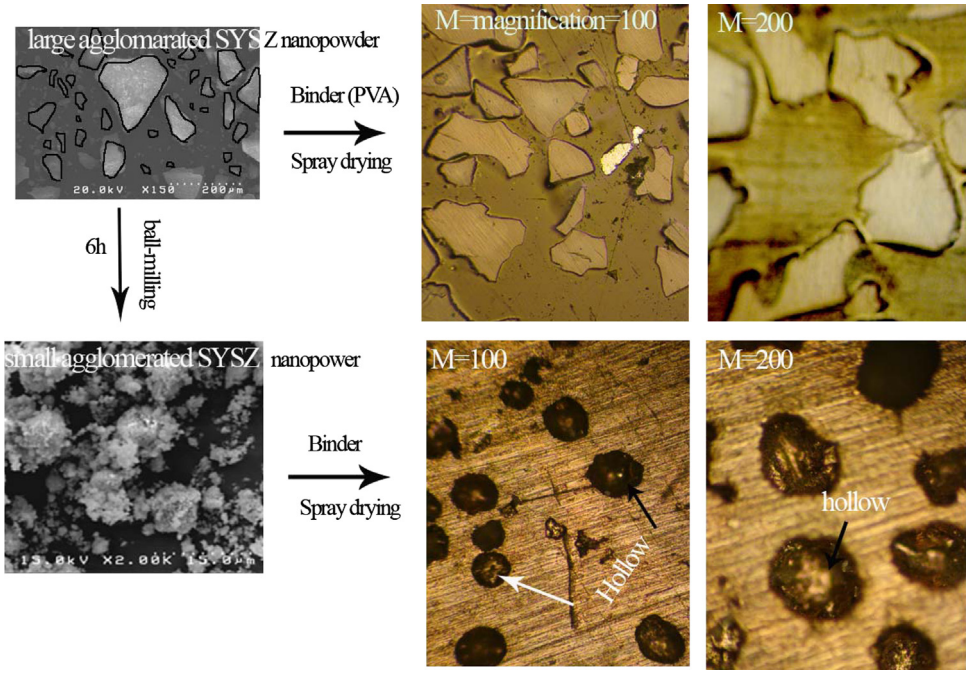

Fig. 4. The effect of ball milling treatment on the resulted SD granules. (Left images: SEM images of nanopowder; right image is optical images of resulted granules.).

drying process. This figure exhibits the typical semi-spherical shape with smooth surfaces of spray-dried agglomerates. The average particle size of this granules was in the range of 55 ± 3 μm. The plasma sprayable powders were of a mean diameter of ~50 μm. So, in terms of average particle size, these granules are suitable for plasma spraying. But, in the case of apparent density, sintering treatment is needed, which will be discussed later. A close look at this figure shows that these granules were hollow (labeled with red line). In addition, some deformed granules were visible in this sample. This heterogeneity can be attributed to liquid-phase separation during the spray-drying operation, possibly due to some surface tension modifier incorporated into the suspension [2,5,13]. However, the untreated nanopowders (SD2, Fig. 2b) showed solid nonspherical morphology with dimensions ranging from 30 μm to 100 μm. SEM images (Fig. 3) of ball milled nanopowders before spray drying showed that big agglomerates in Fig. 1a were broken into small ones. So, after spray drying of this powder (see Fig. 4), spherical granules were obtained. The irregular and angular morphologies of SD2 powder resulted from original angular nature of as-obtained SYSZ nanopowders (see Fig. 4) prepared with the polymeric sol–gel method [1]. In the case of ball-milled SYSZ nanopowders, semi-spherical granules were obtained. It was due to presence of dispersed SYSZ nanoparticles in its suspension. For the non-ball milled SYSZ nanopowders, the surface tension would not pull the droplets into a sphere or semi-sphere because of existing large agglomerate in the suspension. Furthermore, high magnification SEM images (inset of Fig. 2a and b) showed that the diameter of nanoparticles was not changed in comparison with the original SYSZ nanopowders.

Furthermore, agglomerates apparent specific mass and flowability were determined for both SD1 and SD2 granules. The value of the first parameter obtained for the SD2 (solid granules, 900 kg/m^3) powders was higher than the SD1 (hollow granules, 560 kg/m^3) powders. However, SD1 (0.39 g/s) granules showed a better flow rate than SD2 ones (0.30 g/s) due to their smooth surface and regular shape [5,6]. Researchers have reported [22] that spray-dried powder with apparent specific mass > 1700 kg/m^3 and mean particle size > 20 μm could be directly processed for plasma spray coating without further densification. Another paper states that the apparent specific mass of the agglomerates of APS spray-dried powders could range widely from less than 1000 kg/m^{3}to 2000 kg/m^3 [23]. Indeed, the feedstocks do not meet the demands for plasma spraying after granulation. In the next section, it is explained how the apparent density of this granule can be improved by calcination (heat treatment) process.

The TGA was used to assign calcinations temperature, as shown in Fig. 5. In Fig. 5a, the mass loss before 300 °C and 300–570 °C was due to the evaporation of deionized water and decomposition of PVA (polyvinyl alcohol), respectively. The phase transformation of ZrO_2 could easily take place from monoclinic to tetragonal at the temperature of 950–1150 °C [1,21], but the ZrO_2 used in this experiment was stabilized by scandia and yttria. So, its phase transformational temperature was not explicit. At 1181 °C, the Y_2O_3 was dissolved out from YSZ solid solution, and then the phase transformation of ZrO_2 took place [24]. So, the maximum sintering temperature was set at 1050 °C (< 1181 °C), and holding time was 1.0 h (Fig. 5b). After sintering at 1050 °C, the apparent density of SD1 and SD2 granules was increased from 560 and 900 kg/m^3 to 810 and 1000 kg/m^3, respectively. By the way, because of crystal growth more than 100 nm (obtained by SEM image, not shown here) of SYSZ granules, the calcination temperature, was kept up to 800 °C.

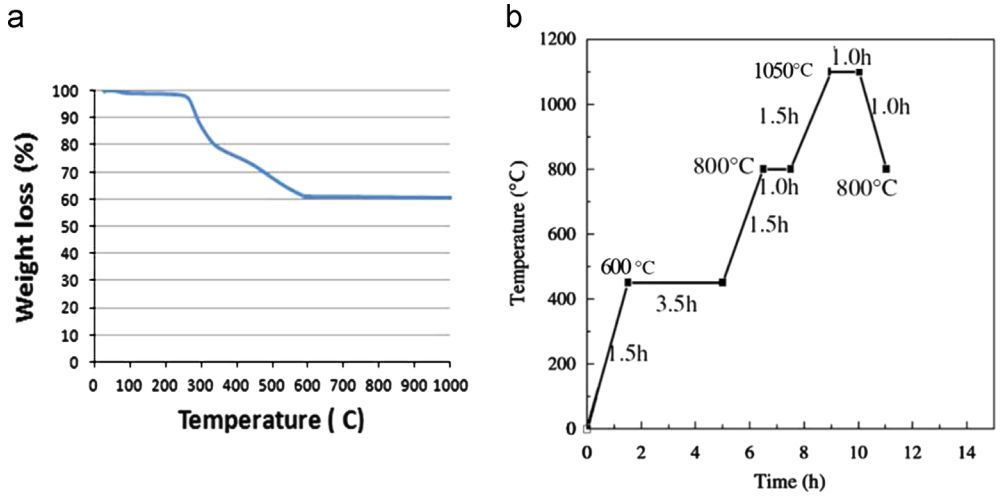

Fig. 5. TGA of granules prepared with 5 wt% binder (a) and (b) heat treatment process.

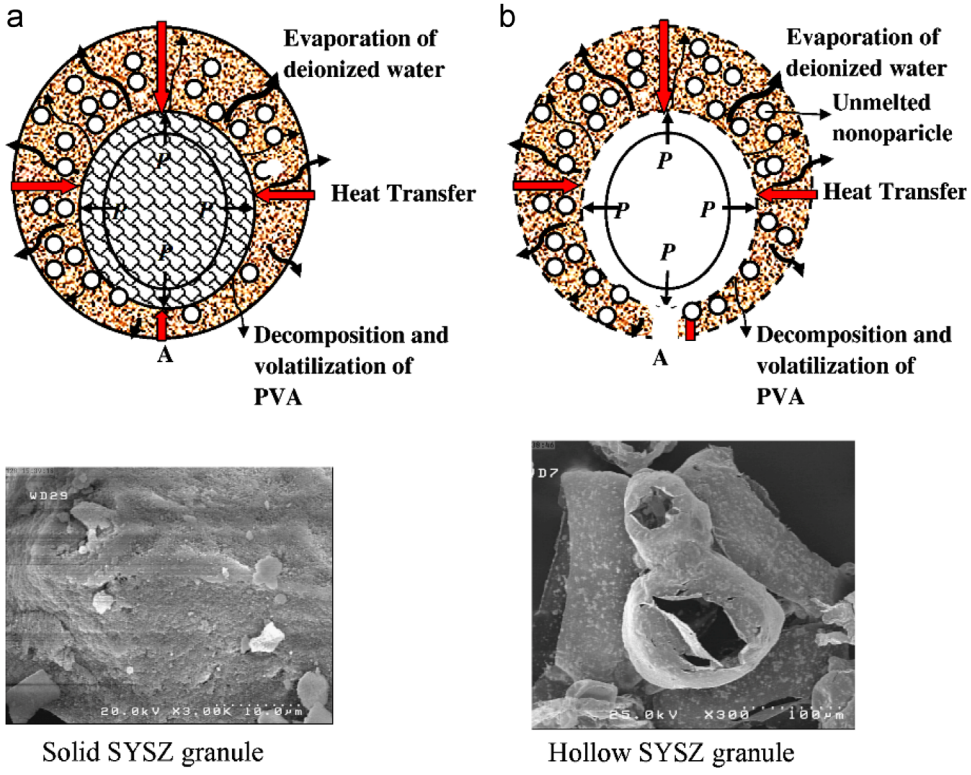

Scheme 1. Schematic illustration of heat transfer of granulated particle in spray drying and calcination process [24].

Scheme 1 shows the illustration of heat transfer and mass loss for granulated particle in spray drying and calcination process. A spherical shell can be created inside the droplet with the synergistic effect of materials and energy. The heat transferred to the interior of droplet from the surface is transferred by thermal conduction, which can be expressed in the following equation,

$$\frac{\partial(\rho C_p T)}{\partial t} = \frac{1}{r^2}\frac{\partial}{\partial r}\left(kr^2\frac{\partial T}{\partial r}\right), \quad 0 \le r \le R(t), \quad t > 0 \tag{1}$$

where, T is the temperature for different time (K), k is the thermal conductivity (W/m^2 K), ρ is the density (g/ml), C_p is the heat capacity (J/mol K), $R(t)$ is the radial of the particle, and r is the radial position. It is assumed that k is the independent of the radial position and time.

$$k = \text{constant} \neq f(r,t) \tag{2}$$

thus, Eq. (1) can be written as,

$$\frac{\partial T}{\partial t} = \alpha\frac{1}{r^2}\frac{\partial}{\partial r}\left(r^2\frac{\partial T}{\partial r}\right), \quad 0 \le r \le R(t), \quad t > 0 \tag{3}$$

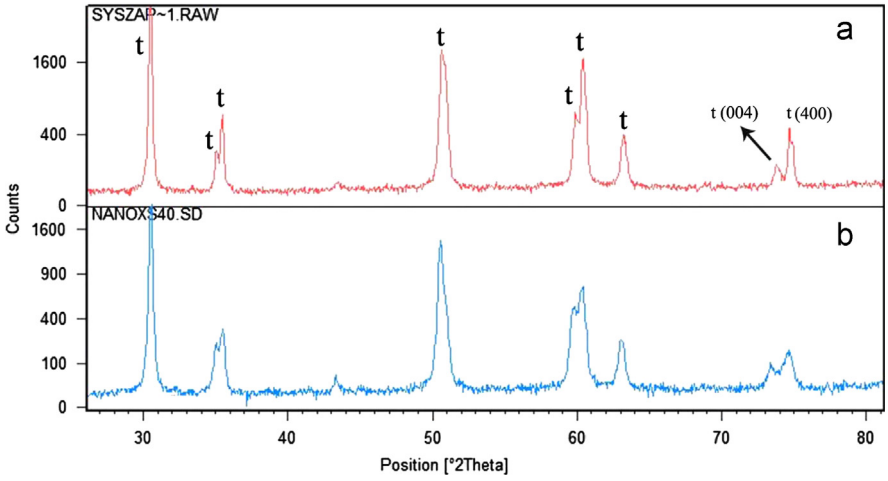

Fig. 6. XRD patterns of APS coating from SD2 (a) and commercial YSZ (b) granules.

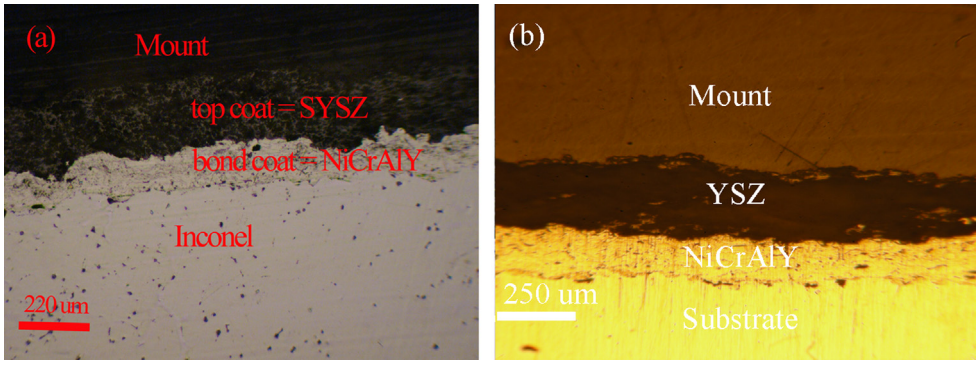

Fig. 7. The optical images of polished cross section of SD2 (a, solid) and commercial YSZ (b, porous) coatings.

where, $\alpha = k/\rho C_p$ is the thermal diffusivity. The heat transfer process can be expressed as following formula in short:

$$\varphi = kA\Delta T \tag{4}$$

where, φ is the heat flow (W), k is the thermal conductivity (W/m^2 k), A is the contact area (m^2), and ΔT is the difference of temperature (K). So, the deionized water and polymer (PVA) can be decomposed and evaporated in the following forms:

$$\text{Polymer}: \quad \frac{\partial c_p}{\partial t} = D\frac{1}{r^2}\frac{\partial}{\partial r}\left(r^2\frac{\partial c_p}{\partial r}\right), \quad 0 \le r \le R(t), \quad t > 0 \tag{5}$$

$$\text{Deionized water}: \quad \frac{\partial c_w}{\partial t} = D\frac{1}{r^2}\frac{\partial}{\partial r}\left(r^2\frac{\partial c_w}{\partial r}\right), \quad 0 \le r \le R(t), \quad t > 0 \tag{6}$$

where, D is binary diffusion coefficient [24]. According to the TGA analysis, the evaporation temperature of deionized water was occurred at 200–295 °C, and the decomposition and volatilization temperature of polymer (PVA) was in temperature range 300–571 °C. In the spray drying process, the inlet temperature is about 225–235 °C. Nearly all the deionized water can be evaporated, and most polymers are retained. The inter granules cannot shrink at the temperature of 225–235 °C, so the spherical surface is smooth (Scheme 1a). In the following heat treatment process, the residual deionized water and polymer (PVA) can be decomposed and volatilized at higher temperature (higher than 570 °C). When the temperature reaches to 800 °C, the nano-granules can grow and the big pores or voids begin to close on the surface. However, some residual submicron pores or voids cannot be closed by calcination. The nano-granules or surface pore shrink leading to coarse surface. It is assumed that the adhesive strength of nano-granules is independent of position (r) in the same particle. The heat transfer can lead to the increment of air pressure in the cavity of particles. The thin zone (Scheme 1b) can firstly reach the limitation of adhesive strength among granulated particles, and then the hollow SYSZ sphere is broken at the position of A.

3.3. APS coatings from agglomerated feedstock

For comparison of coating porosity and percent of non-melted area, the nanostructured porous YSZ granules were purchased from Inframat (Nanox S4007) company. The morphology of this powder was reported by other researchers [6,7]. Coatings were obtained from the following spray-dried feed stocks: commercial porous granules (Nanox S2400) and solid irregular granules (non-ball-milled, SD2). Based on the XRD pattern shown in Fig. 1d, the nanostructured SYSZ powder contained T′ phase (the non-transformable tetragonal

zirconia). Accordingly, the SYSZ coatings fabricated from non-ball milled nanopowder contained only T′ phase (Fig. 6), because molten part of powder, due to rapid cooling, formed T′ phase and non-molten part retained the T′ phase [7,9]. The same results were obtained from plasma spraying of commercial porous granules [7,9].

Optical and SEM images of polished cross section of both coatings were shown in Fig. 7. Fig. 7a–d shows the optical image of the nano-YSZ and SYSZ coating polished cross-section, which appears to be well bonded to the substrate. It should be noted that the thickness of top coating is quite heterogeneous. The thickest section is up to 265 μm, while the thinnest region is only 220 μm. Fig. 8 shows FESEM micrographs of the coatings obtained from the SD2 (solid) powders at different magnifications. The coatings displayed the typical microstructure of APS coatings deposited from nanostructured powders as used here [6,7]. The literature indicates that such coating microstructures basically comprise two clearly differentiated zones, yielding a two-scale structure [6,7,25]. One coating region, which was completely melted (marked M in Fig. 8), consisted mainly of submicrometre-size grains of SYSZ. The other coating region, which was only partly melted (marked PM), largely retained the microstructure of the starting nanopowder, thus principally making up nanometre-sized grains of SYSZ (nanozone). The particle size of this splat-quenched SYSZ was extremely small (20–70 nm, inset Fig. 8c). Moreover, fractured cross-section of both coatings showed that splats had microcolumnar-grain structure. This columnar structure was formed by directional solidification at rapid cooling [25,26]. The cross section morphology of nanostructured YSZ coating, produced from commercial YSZ granules (Nanox S4007, Inframat Company, USA) was reported in other research [6,7]. No significant differences were observed between the micrographs of SYSZ and YSZ nanocoating. The contribution of this two-scale coating structure to the enhancement of coating properties can be compared to the conventional micrometre-sized coatings, as clearly shown elsewhere [6,7]. However, most studies have focused on the impact of plasma spraying variables on the amount of the preserved nanostructure area, while the role of granulated feedstock has hardly been addressed. In view of the above, the total void content of the coatings, as well as the amount of semi-molten areas (partially molten area, PM), was estimated by image analysis at 200, 500 and 1000 magnifications (Fig. 9). These magnifications enabled void content and semi-molten nanozone areas to be estimated for comparative purposes. However, voids could not be readily distinguished from semi-molten areas because both areas were detected as black particles. To perform this identification, the binaries image of the sample was first obtained in black and white colors. Subsequently, the assignment of the distribution of black areas was made as follows: voids plus semi-melted area (total area of black particles), voids (total area of black particles minus areas of black particles with a surface area greater than 150 μm^2), and semi-melted areas (area of black particles with a surface area greater than 150 μm^2). The 150 μm^2 threshold for the semi-molten areas was assigned after microscopic observation of many of these areas. The void content data at 500 magnifications are detailed in Table 1. The results at 200 magnifications were very similar to those obtained at 500 and 1000 magnifications, but a better differentiation was observed between the voids and the semi-molten areas at 500 and 1000 magnifications. These results showed that solid granulates (Fig. 9a and b) obtained from non-ball-milled nanopowder seemed to lead less porous coatings in which the amount of semi-molten areas was also reduced more than the YSZ coating (Fig. 9c and d). These findings showed that controlling feedstock characteristics enabled the amount of voids and semi-melted areas to be appropriately adjusted.

3.4. Thermal insulation capability

The main task of the TBCs is to reduce the heat transfer to the hot-section metal components. Therefore, the thermal insulation capability is considered as one of the most significant factors in evaluating the performance of TBCs. In this

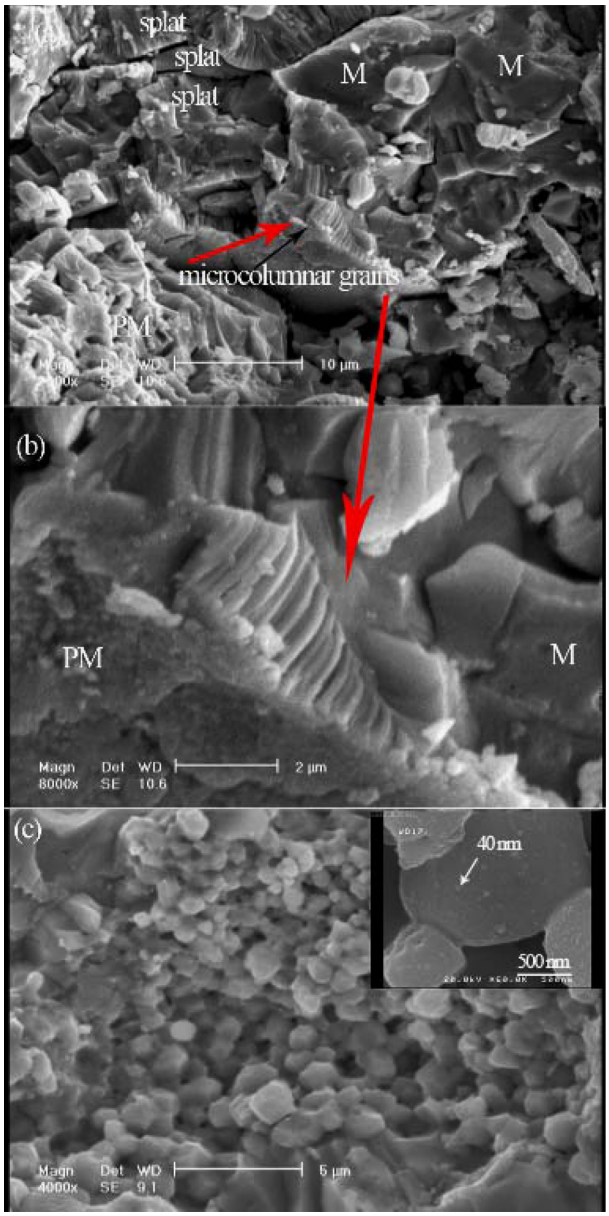

Fig. 8. SEM (a–c) micrographs of fracture section of SYSZ with different magnifications plasma sprayed from SD2 (solid) powder.

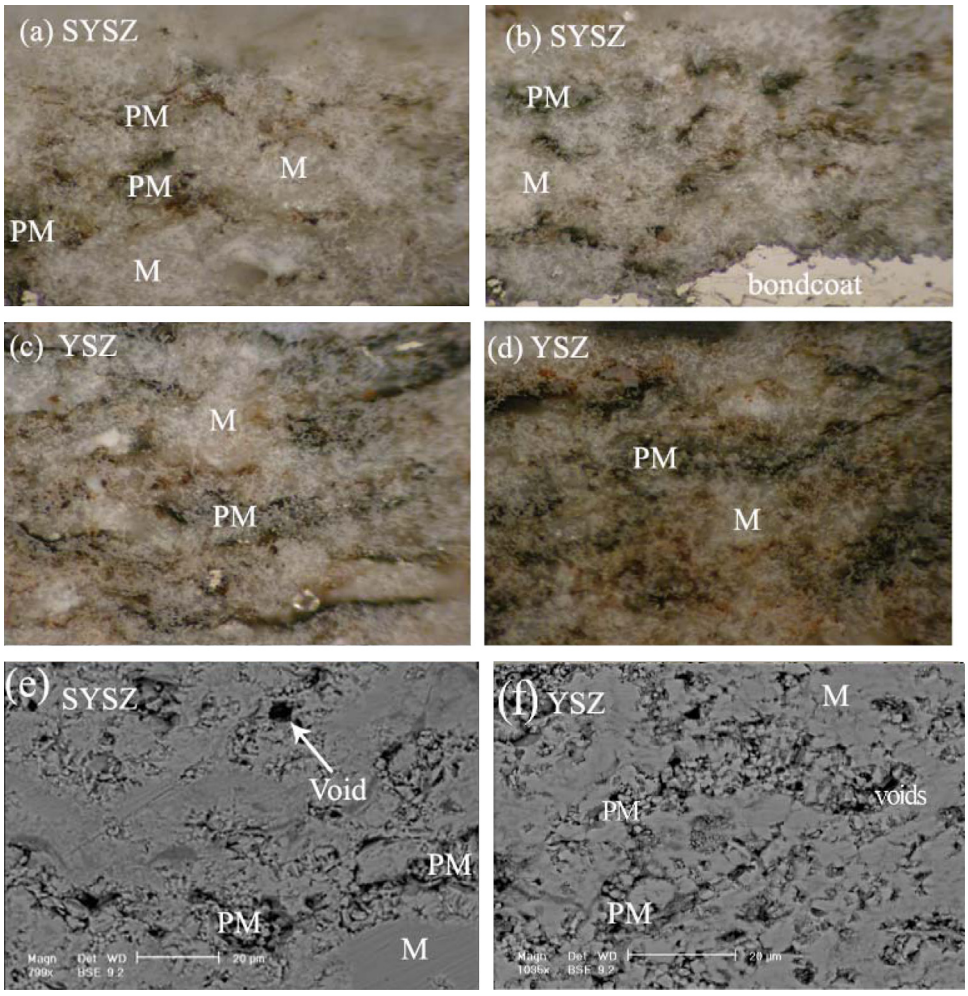

Fig. 9. Optical (a–d) and back scattered SEM (e and f) images of cross section of SYSZ and YSZ APS coating, with different magnifications (magnification of optical image is equal to 200).

Table 1
Voids and partially melted areas of APS coatings determined by the image analysis software.

Coating sample	Voids+PM areas (%)	Voids (%)	PM areas (%)
YSZ	36 ± 4	4 ± 1	32 ± 3
SD2 (solid SYSZ granules)	27 ± 3	7 ± 2	20 ± 4

study, the thermal insulation capability of TBCs was evaluated by the temperature drop across TBCs.

Fig. 10 presents the recorded heating temperature curves of the electric furnace (T_0), backside of substrate coated with TBC (T_1), and the backside of substrate without TBC (T_2) versus time for the commercial (curve a) and SD2 (curve b) coatings. Based on the results, thermal insulation capability for SD2 (SYSZ, solid granules) and YSZ (porous granules) TBCs was found to be 54 °C and 158 °C, respectively. It should be noted that the low thermal insulation capability value of SYSZ coating was due to contamination of SYSZ nanocoating with Fe element during spray drying of SYSZ suspension (Fig. 11). In future work, pure SYSZ granules will plasma sprayed that their result will report in other research. Furthermore, according to the results of semi-empirical calculations, it can be concluded that the thermal conductivity decreases with an increase in ionic radius of dopants, caused by the reduction in the mean free path of phonons and the presence of excess grain boundaries [15,16]. Thus, another reason for the lower value of SYSZ thermal insulation capability is the ionic radius of Sc^{3+} (0.081 nm) was less than radius of Y^{3+} cations (0.093 nm). Furthermore, nanostructured ceria stabilized zirconia (CSZ), with 200 and 400 μm thickness, shows thermal insulation value of 92 °C and 155 °C, respectively. This demonstrates that the thermal insulation capability of the nanostructured TBC prepared from porous granules, as compared to the one prepared from plasma spraying of solid granules, was higher. Indeed, heat transfer from the plasma to the nanoparticles differed completely in nanostructured porous agglomerates from that in irregular solid ones. This is basically because heat diffusion is slower in comparison to dense agglomerates [4,6]. So, this caused to produce different partially and non-melted area (nanozone) and thermal insulation capability of both coatings. Moreover, Lima et al. [6] showed that in the case of TBC, the void microstructures were determined by

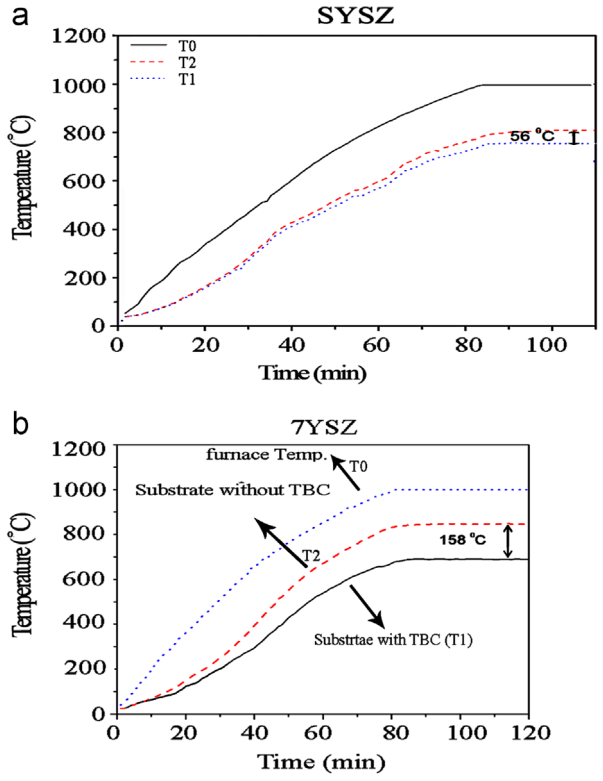

Fig. 10. The heating temperature curves of the electric furnace (T_0), backside of substrate coated with TBC (T_1) and backside of substrate without TBC (T_2) versus time for the SD1 (SYSZ, solid granules) (a) and commercial porous YSZ (b) coatings.

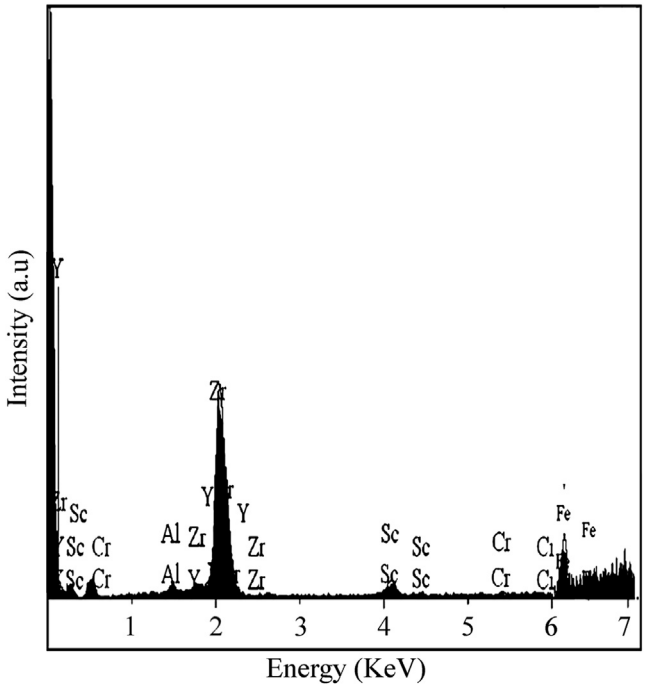

Fig. 11. The EDS analysis of SYSZ nanocoating.

both the spraying conditions and the feedstock material. Moreover, Diez and Smith [27] and Wigren et al. [28] explained the effect of powder characteristics in TBC properties. Thus, controlling and optimizing powders morphology appear to be the first step for enhancing the thermal behavior of plasma sprayed TBC.

The ability of thermal insulation of plasma-sprayed SYSZ and YSZ coatings can be attributed to characteristics of crystal structure and microstructure that result from the spraying process. The microstructure of plasma-sprayed TBCs contained a network of microcracks and porosities providing low thermal conductivity through thickness [6,29–33]. The plasma-sprayed ceramic conventional coatings exhibited a bimodal distribution of porosity including coarse pores resulting from incomplete filling of interstices among previously deposited particles and fine pores resulting from incomplete contact between the two piled up splats [6]. It can be seen from Fig. 8 that the nanostructured SYSZ coating exhibited a trimodal distribution of porosity, including coarse pores resulting from incomplete filling of interstices among previously deposited particles and fine pores resulting from incomplete contact between two piled up splats, as well as the nanoporosities associated with the nanozones (Fig. 8c). Therefore, the presence of this source of porosity in nanostructured coating (porous YSZ granules show more nanozone percent than solid SYSZ ones) increased the thermal insulation value.

4. Closing remarks and conclusions

The fabrication of high-quality sprayable coatings with nano-sized powders was the research focus, but the nanopowders used to make ceramic coatings with low flowability and densities have led to the worse properties of coatings. So, this work demonstrated a simple and industrial method for the upgrading of a nano-sized SYSZ nanopowder into granules by spray drying which was followed by consolidation thermal treatment. Semi-spherical non-dusty granules with good flow properties could be produced in a spray dryer with 5 wt% PVA. These granules had a smooth surface that showed why this powder had a good flowability. All coatings displayed a two-scale microstructure with partly molten agglomerates that retained the initial nanostructure of the feedstock surrounded by a fully molten matrix. The amount of semi-molten areas, as one of the source of porosity in APS nanocoating, could be regulated by adjusting the feedstock characteristics. Results showed that porous YSZ granules yielded coatings with higher porosity and thermal insulation capability than solid ones.

Acknowledgments

The authors would like to acknowledge Malek Ashtar University of Technology, Department of material engineering, for the financial support. One of the authors would like to dedicate this work to her dear daughter, Sara Loghman, for her birth day. I have special thanks from IBM institute (Mr. bani) for help in zeta potential analysis. The author have special thanks from Dr. F. Davar for use full guide in improvement of this article.

References

[1] M.R. Loghman-Estarki, R. ShojaRazavi, H. Edris, Synthesis of SYSZ nanocrystal via new wet chemical method, Current Nanoscience 8 (2012) 767.

[2] W.B. Gong, C.K. Sha, D.Q. Sun, W.Q. Wang, Microstructures and thermal insulation capability of plasma-sprayed nanostructured ceria stabilized zirconia coatings, Surface and Coatings Technology 201 (2006) 3109.

[3] A.J. Allen, G.G. Long, H. Boukari, J. Ilavsky, A. Kulkarni, S. Sampath, H. Herman, A.N. Goland, Microstructural characterization studies to relate the properties of thermal spray coatings to feedstock and spray conditions, Surface and Coatings Technology 146–147 (2001) 544.

[4] P. Fauchais, G. Montavon, R.S. Lima, B.R. Marple, Engineering a new class of thermal spray nano-based microstructures from agglomerated nanostructured particles, suspensions and solutions: an invited review, Journal of Physics D: Applied Physics 44 (2011) 093001.

[5] W.J. Walker, J.S. Reed, S.K. Verma, Influence of slurry parameters on the characteristics of spray-dried granules, Journal of the American Ceramic Society 82 (1999) 1711.

[6] R.S. Lima, A. Kucuk, C.C. Berndt, Integrity of nanostructured partially stabilized zirconia after plasma spray processing, Materials Science and Engineering A313 (2001) 75.

[7] H. Jamali, R. Mozafarinia, R. Shoja Razavi, R. Ahmadi-Pidani, M. R Loghman-Estarki, Fabrication and evaluation of plasma-sprayed nanostructured and conventional YSZ thermal barrier coatings, Current Nanoscience 8 (2012) 402.

[8] X.J. Ning, C.X. Li, C.J. Li, G.J. Yang, Effect of powder structure on microstructure and electrical properties of plasma-sprayed 4.5 mol% YSZ coating, Vacuum 80 (2006) 1261.

[9] R. Peter, B.Strutt, lt. Kear, R.F. Boland, Method of Manufacturing of Nanostructred feeds, US Patent No. 6,025,034.

[10] E. Sizgek, J.R. Bartlett, M.P. Brungs, Production of titanate microspheres by sol–gel and spray-drying, Journal of Sol-Gel Science and Technology 13 (1998) 1011.

[11] M.R. Loghman-Estarki, M. Hajizadeh-Oghaz, H. Edris, R. Shoja Razavi, Comparative studies on synthesis of nanocrystalline Sc_2O_3–Y_2O_3 doped zirconia (SYDZ) and YSZ solid solution via modified and classic Pechini method, Crystal Engineering Communication, 2013, http://dx.doi.org/10.1039/c3ce40288f.

[12] A. Pattanayak, A. Subramanian, Production of meso- and giga-porous zirconia particles—an improved multi-step particle aggregation process Abhinandan Pattanayak, Anuradha Subramanian, Powder Technology 192 (2009) 359.

[13] K. Masters, Drying of droplets/sprays, in: Spray Drying Hand book, 4th edn., John Wiley & Sons, New York347–348.

[14] T. Fengqiu, H. Xiaoxian, Z. Yufeng, G. Jingkun, Effect of dispersants on surface chemical properties of nanozirconia suspensions, Ceramics International 26 (2000) 93.

[15] J.A. Eastman, U.S. Choi, S. Li, G. Soyez, L.J. Thompson, R.J. Dimelfi, Novel thermal properties of nanostructured materials, Materials Science Forum 629 (1999) 312.

[16] H.S. Yang, G.R. Bai, L.J. Thompson, J.A. Eastman, Interfacial thermal resistance in nanocrystalline yttria-stabilized zirconia, Acta Materialia 50 (2002) 2309.

[17] A. Mukherjee, B. Maiti, A.D. Sharma, R.N. Basu, H.S. Maiti, Correlation between slurry rheology, green density and sintered density of tape cast yttria stabilised zirconia, Ceramics International 27 (2001) 731.

[18] K. Prabhakaran, A. Melkeri, N.M. Gokhale, T.K. Chongdar, S. C. Sharma, Direct coagulation casting of YSZ powder suspensions using MgO as coagulating agent, Ceramics International 35 (2009) 1487.

[19] W. Li, L. Gao, Nano ZrO_2–Y_2O_3 particles processing by heating of ethanol-aques salt solution, Ceramics International 27 (2001) 543.

[20] (a) ASTM B0212-99, Test Method for Apparent Density of Free-Flowing Metal Powders Using the Hall flowmeter funnel;
(b) ASTM B 213–03, Standard Test Method for Flow Rate of Metal Powders.

[21] M.R. Loghman-Estarki, R. Shoja Razavi, H. Edris, Synthesis and thermal stability of ZrO_2, Re–Sc, Y nanocrystals, Defect and Diffusion Forum 334 (2013) 60.

[22] X.Q. Cao, R. Vassen, S. Schwartz, W. Jungen, F. Tietz, D. Stöever, Spray-drying of ceramics for plasma-spray coating, Journal of the European Ceramic Society 20 (2000) 2433.

[23] E. S´anchez, A. Moreno, M. Vicent, M.D. Salvador, V. Bonache, E. Klyatskina, I. Santacruz, R. Moreno, Preparation and spray drying of Al_2O_3–TiO_2 nanoparticle suspensions to obtain nanostructured coatings by APS, Surface and Coatings Technology 205 (2010) 987.

[24] Z. Pan, Y. Wang, X. Sun, Fabrication and characterization of spray dried Al_2O_3–ZrO_2–Y_2O_3 powders treated by calcining and plasma, Powder Technology 212 (2011) 316.

[25] X. Jiang, C. Liu, M. Liu, H. Zhu, Influence of heat treatment on nanocrystalline zirconia powder and plasma-sprayed thermal barrier coatings, Transactions of Nonferrous Metals Society 20 (2010) 2272.

[26] C. Liu, Z. Zhang, X. Jiang, M Liu, Z. Zhu, Comparison of thermal shock behaviors between plasma-sprayed nanostructured and conventional zirconia thermal barrier coatings, Transactions of Nonferrous Metals Society 19 (2009) 99.

[27] P. Diez, R.W. Smith, The influence of powder agglomeration methods on plasma sprayed yttria containing, Journal of Thermal Spray Technology 2 (1993) 165.

[28] J. Wigren, J.-F. de. Vries, D. Greving, Effects of powder morphology, microstructure, and residual stresses on thermal barrier coating thermal shock performance, in: C.C. Berndt (Ed.), Thermal Spray: Practical Solutions for Engineering Problems, ASM International, OH, USA, 1996, pp. 855–861.

[29] I.O. Golosnoy, A. Cipitri, T.W. Clyne, Heat transfer through plasma-sprayed thermal barrier coatings in gas turbines: a review of recent work, Journal of Thermal Spray Technology 18 (2009) 809.

[30] M. Salavati-Niasari, M. Dadkhah, F. Davar, Synthesis and characterization of pure cubic zirconium oxide nanocrystals by decomposition of bis-aqua, tris-acetylacetonato zirconium(IV) nitrate as new precursor complex, Inorganica Chimica Acta 362 (2009) 3969.

[31] M. Salavati-Niasari, M. Dadkhah, F. Davar, Pure cubic ZrO_2 nanoparticles by thermolysis of a new precursor, Polyhedron 28 (2009) 3005.

[32] M. Hajizadeh Oghaz, R. Shoja Razavi, M.R. Loghman-Estarki, R. Ghasemi, Optimization of morphology and particle size of modified sol–gel synthesized YSZ nano powder using Taguchi method, Journal of Nano Research 21 (2013) 65.

[33] F. Davar, A. Hassankhani, M.R. Loghman-Estarki, Controllable synthesis of metastable tetragonal zirconia nanocrystals using citric acid assisted sol–gel method, Ceramics International 39 (2013) 2933.